Materials Science-Poland, 35(2), 2017, pp. 265-274
http://www.materialsscience.pwr.wroc.pl/
DOI: 10.1515/msp-2017-0037

DE GRUYTER OPEN

Gas-sensing properties and *in-situ* diffuse-reflectance Fourier-transform infrared spectroscopy study of diethyl ether adsorption and reactions on SnO_2 film

NING WANG[1], KAIJIN HUANG[1,2*], JIAN SONG[1]

[1]State Key Laboratory of Materials Processing and Die & Mould Technology, Huazhong University of Science and Technology, Wuhan 430074, P.R. China

[2]State Key Laboratory of Advanced Technology for Materials Synthesis and Processing, Wuhan University of Technology, Wuhan 430070, P.R. China

Diethyl ether is a common industrial reagent and medical anesthetic. It is necessary to carry out real-time monitoring of this molecule due to its harmful effects on human health. In this paper, a highly sensitive diethyl ether SnO_2 gas-sensing material has been prepared by a sol-gel method. The gas sensitivity was tested by a home-made gas-sensing equipment. The surface adsorption and reaction processes between the SnO_2 gas-sensing film and the diethyl ether have been studied by in situ diffuse-reflectance Fourier-transform infrared spectroscopy (DRFT-IR) at different temperatures. The results show that the SnO_2 gas-sensing material has high sensitivity to diethyl ether, and the lowest detection limit can reach 1 ppm. Furthermore, ethyl ($CH_3CH_2\bullet$), oxoethyl ($CH_3CH_2O\bullet$), ethanol (CH_3CH_2OH), formaldehyde (HCHO), acetaldehyde (CH_3CHO), ethylene (C_2H_4), H_2O and CO_2 surface species are formed during diethyl ether adsorption at different temperatures. A possible mechanism of the reaction process is discussed.

Keywords: *gas sensitivity; SnO_2 film; diethyl ether; in situ DRFT-IR*

1. Introduction

Diethyl ether is a common organic solvent that is widely used in the fields of diesel engines, agriculture, and food, chemical, biological, pharmaceutical, and medical industries [1–4]. Due to its volatility, pungent odor, anesthetic effect, flammability, and explosive nature, diethyl ether creates a great risk to human health and safety. Prolonged inhalation of even low concentration can lead to headache, dizziness, proteinuria, disease of growth in quantity of red blood cells and even death [5–7]. Consequently, the maximum permissible concentration-time-weighted average (PC-TWA) and permissible concentration-short-term exposure limit (PC-STEL) for diethyl ether are 300 mg/m^3 (91 ppm) and 500 mg/m^3 (151.1 ppm), respectively, in China [5]. Therefore, it is necessary to carry out real-time monitoring of this compound.

To date, many methods have been devised for the detection of diethyl ether at the ppm or ppb level. Gas chromatography (GC) [8], GC/MS [9], surface acoustic wave [10], gas test-tube [11], chemiluminescence (CL) and cataluminescence (CTL) methods [9, 12] have been used to detect ppm and/or ppb grade diethyl ether. However, these methods are associated with various disadvantages, being either expensive, or time-consuming, requiring complex experimental apparatus or large instrument volume, or involving toxic solvents or reagents [8–12]. On the other hand, gas sensors based on metal oxide semiconductors, like SnO_2, ZnO and Fe_2O_3 have attracted much attention due to their unique features, such as low cost, high sensitivity, fast response, relative simplicity and portability [13–15].

It is well known that SnO_2 is widely used as a gas-sensing material. Many literature reports [16–21] have highlighted the excellent gas-sensing properties of SnO_2. For example, Ohgaki et al. [16] reported that the sensitivities of a PLD-grown SnO_2

*E-mail: huangkaijin@hust.edu.cn

© 2017. This is an open access article distributed under the Creative Commons Attribution-NonCommercial-NoDerivatives 3.0 License. (http://creativecommons.org/licenses/by-nc-nd/3.0/)

sensor to 1000 ppm NO_2 and 1 % H_2 were 2 and 1 at 350 °C, respectively. Liu et al. [17] reported that the sensitivities of an SnO_2 sensor to 10 ppm, 20 ppm, 30 ppm, 40 ppm and 50 ppm ethanol were 18.8, 33.3, 42.7, 51.8 and 60.5, respectively. He et al. [18] reported that the sensitivities of a porous SnO_2 nanotube sensor to 100 ppm ethanol and acetone were 130 and 126 at 200 °C, respectively. Wang et al. [19] reported that the sensitivity of an SnO_2 nanorod sensor to 1 ppm triethylamine was 3.0 at 350 °C. Hyodo et al. [20] reported that the sensitivity of a mesoporous SnO_2 sensor to 1000 ppm H_2 was 337 at 400 °C. Huang et al. [21] reported that the sensitivity of an SnO_2 nanotube sheet to 100 ppm H_2 was 16.5 at 450 °C.

To the best of our knowledge, there has been no literature report on the sensing of diethyl ether with SnO_2 gas-sensing material, although many reports have been concerned with the sensing of diethyl ether with other materials [22–28]. For example, Wang et al. [22] studied the gas sensitivity of a P(St-AM)@Ag sensor and found that the gas sensitivity of about 3.12 was achieved at 16 °C. The lowest concentration detection limit and the response/recovery times were not specified. Ren [23] studied the diethyl ether vapor-sensing properties of SnO_2-0.005 % palladium asbestos, SnO_2-0.005 % CeO_2 and ZnO-0.05 % rare earth oxide (REO) sensors. The results showed that the gas sensitivities (I_g/I_a) were 3.2, 0.33 and 170 respectively, at a diethyl ether concentration of 0.05 %. Again, the lowest concentration detection limit and the response/recovery times were not specified. Slobodian et al. [24] reported diethyl ether vapor-sensing properties of various multi-walled carbon nanotube (MWCNT)-based sensors, specifically based on pure MWCNTs, oxidized MWCNTs, and sonicated MWCNTs. The gas sensitivities ($(R_g - R_a)/R_a \cdot 100$ %) were about 21 %, 28 % and 2.6 %, respectively, at 25 °C at a volume concentration of 70.9 %. The response times were 90 s to 130 s and the recovery times were 200 s to 260 s. Ma et al. [25] studied the diethyl ether vapor-sensing properties of an Ag/α-Fe_2O_3 based sensor. The gas sensitivity was 3.0 at 260 °C and 100 ppm, and the response and the recovery times were 5 s and 6 s, respectively. Zhao et al. [26] reported diethyl ether gas sensitivities of SiC films as 1.1 (at 50 ppm) and 1.3 (at 400 ppm) at 250 °C. Aizawa et al. [27] reported diethyl ether gas sensitivity of a PP-HMDSO film as 4.5. Gui et al. [28] reported that the gas sensitivity of a Pd doped WO_3 sensor to 2240 ppm diethyl ether was about 10.

In this study, SnO_2 gas-sensing material has been prepared by sol-gel method and deployed for sensing of diethyl ether vapor. The adsorption and reactions on the SnO_2 gas-sensing film have been studied by in situ diffuse reflectance Fourier-transform infrared spectroscopy.

2. Experimental

2.1. Preparation and characterization of nano-SnO_2 powder

Nano-SnO_2 powder was prepared by a sol-gel method. An aqueous solution of $SnCl_4$ (0.5 $mol \cdot L^{-1}$) was prepared by mixing $SnCl_4 \cdot 5H_2O$ (10.6242 g) with distilled water (60 mL). An $NH_3 \cdot H_2O$ aqueous solution (3.5 $mol \cdot L^{-1}$) was added dropwise to the aqueous solution under stirring at 50 °C to 60 °C, until the pH value of 2 to 3 was reached. The obtained solution was boiled at 55 °C for 2 h, during which the solution slowly turned into a turbid colloidal solution. After cooling down, the sol was collected from the solution by filtration and washed several times with distilled water and ethanol. After drying at 80 °C for 12 h in a drying oven, the obtained gel powders were ground in a mortar and calcined in a muffle furnace at 500 °C for 2 h to obtain nano-SnO_2 powders. The nano-SnO_2 powders were examined by XRD and FESEM techniques. The results of XRD and FESEM showed that the nano-SnO_2 powders had crystalline rutile structure consisting of spherical crystals with diameters of approximately 10 nm to 20 nm. The detailed characterization of nano-SnO_2 powder was given in our previous paper [29].

2.2. Measurement of diethyl ether gas-sensing properties

A gas-sensing paste was first obtained by grinding. For this purpose, the prepared SnO_2 powder

was mixed and ground with the appropriate amount of organic solution, and ball-milled in an agate mortar for 3 h. A screen-printing technique was then used to print the paste onto an alumina substrate with pre-printed Au interdigital electrodes. Thereafter, the alumina substrate with the printed SnO_2 paste (60.0 wt.% SnO_2, 21.24 wt.% terpineol, 10.62 wt.% butyl-carbitol-acetate, 3.54 wt.% di-n-butyl phthalate, 2.4 wt.% ethylcellulose, 1.6 wt.% Span 85, 0.4 wt.% butyrolactone, and 0.2 wt.% hydrogenated castor oil) were sintered at 550 °C for 3 h. Finally, the alumina substrate with the printed SnO_2 gas-sensing material was aged at 250 °C for 3 days in air to enhance the gas-sensing stability. The gas sensitivity of SnO_2 film to diethyl ether was tested with our in-house-constructed equipment. A high throughput test platform for characterization of gas sensitivity was designed and established in our laboratory. The test platform has the advantages such as high throughput (36 test channels), large resistance measurement range (500 Ω to 100 MΩ, and test error less than 5 %), accurate temperature control (within 1 °C), and friendly interface. The gas-sensing material testing platform consisted of a computer, temperature control module, gas path control module, signal conditioning module, and test chamber. The detailed procedure was described in the literature [30]. Gas sensitivity is defined in this paper as $S = R_a/R_g$ [25, 31], where R_a and R_g are the resistances of a sensor in air and in a test gas, respectively.

2.3. *In-situ* DRFT-IR study

The adsorption and reactions of diethyl ether on SnO_2 film were studied by *in-situ* diffuse-reflectance Fourier-transform infrared spectroscopy (DRFT-IR). All spectra were recorded at 350 °C to 400 °C on a VERTEX 70 FT-IR Spectrometer (Bruker) equipped in a liquid-nitrogen-cooled mercury cadmium telluride detector in a range of 3800 cm^{-1} to 1000 cm^{-1} and a diffuse-reflectance accessory containing an environment and temperature controlled reflectance cell equipped with KBr windows. The spectra with a resolution of 4 cm^{-1} were obtained by averaging 128 scans and analyzed using OPUS software. Further details can be found in the literature [32]. A gas stream (30 $mL \cdot min^{-1}$) of 200 ppm diethyl ether was introduced into the cell at 350 °C, 380 °C, or 400 °C, and the spectra were recorded on the pre-treated sample. It should be pointed out that oxygen existed in the 200 ppm diethyl ether during the DRFT-IR test because the dry synthetic air (20 % O_2+ 80 % N_2) was used as the filling gas of the diethyl ether. In addition, according to [33], the initial auto-oxidation temperature of diethyl ether was approximately 389 K and thermal decomposition occurred under an oxygen atmosphere at low temperature. The oxidation reaction pathway of diethyl ether with oxygen was found to occur in three stages: (1) absorption of oxygen and generation of peroxide by diethyl ether; (2) free radical generation by thermal decomposition and (3) complex oxidation reaction by free radicals. So, the catalytic reactions of diethyl ether on the surface of SnO_2 and the thermal decomposition reactions of diethyl ether in the measuring cell existed during the DRFT-IR test. Independently of the kind of reaction, the final reaction products in an atmosphere containing oxygen, were CO_2 and H_2O. Therefore, the products identified by the DRFT-IR spectra should be the comprehensive products of catalytic reactions and thermal decomposition reactions of diethyl ether.

3. Results and discussion

3.1. Gas-sensing properties of SnO_2 sensor arrays

Fig. 1 shows a plot of the effect of operating temperature on the gas sensitivity of SnO_2 sensor to 200 ppm diethyl ether. The gas sensitivity increases with increasing operating temperature, and reaches a maximum value of 113.03 at 380 °C. This phenomenon is very common and can be found in many literature reports [32, 34, 35]. The reason is that the adsorption mode of oxygen molecules changes from physisorption at lower temperature to chemisorption at higher temperature [32].

The amount of chemically adsorbed diethyl ether increases with increasing of working temperature from room temperature. The more

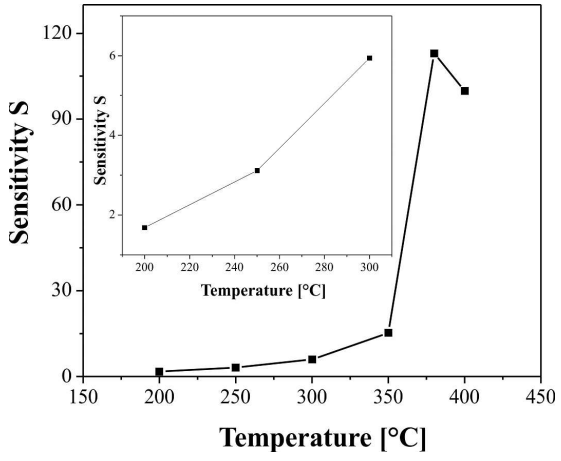

Fig. 1. Effect of operating temperature on the gas sensitivity of the SnO_2 sensor to 200 ppm diethyl ether.

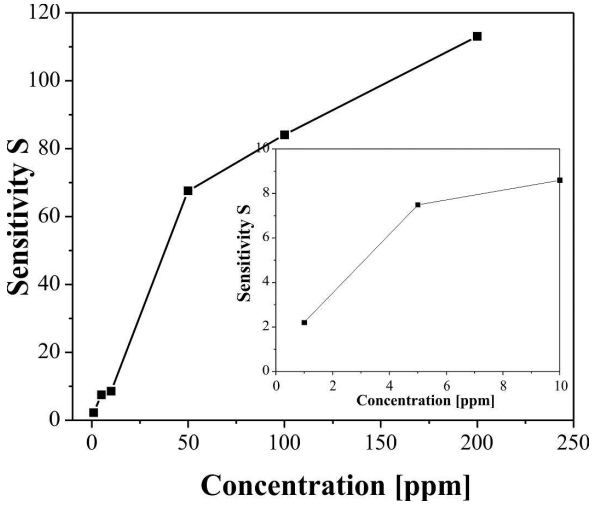

Fig. 2. Gas sensitivity of the SnO_2 sensor vs. diethyl ether concentration (1 ppm to 200 ppm) at 380 °C.

the chemically adsorbed diethyl ether, the more negative oxygen ions consumed, the more free electrons are produced, and the more the resistance of the gas-sensing material decreases. So, the gas sensitivity increases with the increase of working temperature. The adsorption reaches a dynamic equilibrium of absorption-desorption at a certain temperature (380 °C in the present case) because the chemisorption is an exothermic reaction. If the working temperature is increased further, the reactants begin to desorb in large quantities [32]. Hence, beyond 380 °C, the amount of absorbed diethyl ether molecules will progressively decrease, and the balance will move toward desorption, resulting in a decreased gas sensitivity above this temperature (Fig. 1). The reactions of adsorption of O_2 and diethyl ether during this process may be described as follows [36]:

$$O_2(g) \Longleftrightarrow O_2(ads) \tag{1}$$

$$O_2(ads) + e^- \Longleftrightarrow O_2^-(ads) \tag{2}$$

$$O_2^-(ads) + e^- \Longleftrightarrow 2O^-(ads) \tag{3}$$

$$C_2H_5OC_2H_5(ads) + 12O^-(ads) \Longleftrightarrow 5H_2O + 4CO_2 + 12e^- \tag{4}$$

Fig. 2 shows the relationship between the gas sensitivity of the SnO_2 sensor and the concentration of diethyl ether. As shown in Fig. 2, the gas sensitivity is dependent on the concentration of diethyl ether from 1 ppm to 200 ppm, and increases with the increase of the concentration at the optimal operating temperature of 380 °C.

This phenomenon is also very common and can be found in many literature reports [34, 37]. The gas sensitivity of the SnO_2 sensor is 2.19 to 1 ppm at 380 °C, and increases to 113.03 to 200 ppm at 380 °C. That is to say, the lowest detection limit of the SnO_2 sensor to diethyl ether can reach 1 ppm, which meets the demand for real-time monitoring of this molecule [5]. The high gas sensitivity of the SnO_2 sensor may be related to its large specific surface area of 51.6819 $m^2 \cdot g^{-1}$ [29]. As an n-type semiconductor, the SnO_2 surface forms an electron depletion layer when negative oxygen ions are adsorbed thereon at the working temperature. This increases the surface potential barrier and the resistance. When diethyl ether molecules reach the gas-sensing material surface, the adsorbed negative oxygen ions are consumed and free electrons are produced. Hence, the resistance of the material is reduced. In the absence of diethyl ether, the resistance is recovered. The change in resistance thus provides a sensitive means of detection.

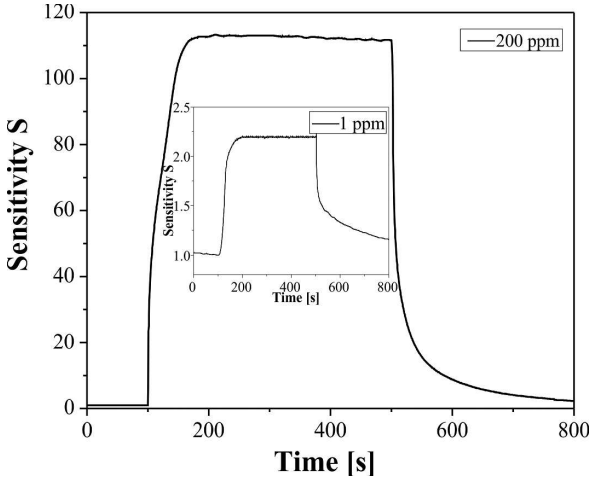

Fig. 3. Response and recovery curve of the SnO_2 sensor to 200 ppm diethyl ether at 380 °C (Inset: corresponding curve at 1 ppm diethyl ether).

In addition, the response and the recovery times of the SnO_2 sensor to 1 ppm and 200 ppm diethyl ether are illustrated in Fig. 3. From Fig. 3, it can be seen that these parameters are 35 s and 125 s, respectively, at 1ppm diethyl ether, and 46 s and 63 s at 200 ppm diethyl ether, respectively.

3.2. *In-situ* DRFT-IR study

Fig. 4 to Fig. 6 show the DRFT-IR spectra obtained at different temperatures (350 °C, 380 °C, and 400 °C) at 200 ppm of diethyl ether. The IR assignments of diethyl ether adsorption on the SnO_2 film and thermal decomposition of ethyl ether at different temperatures are given in Table 1 [38–53].

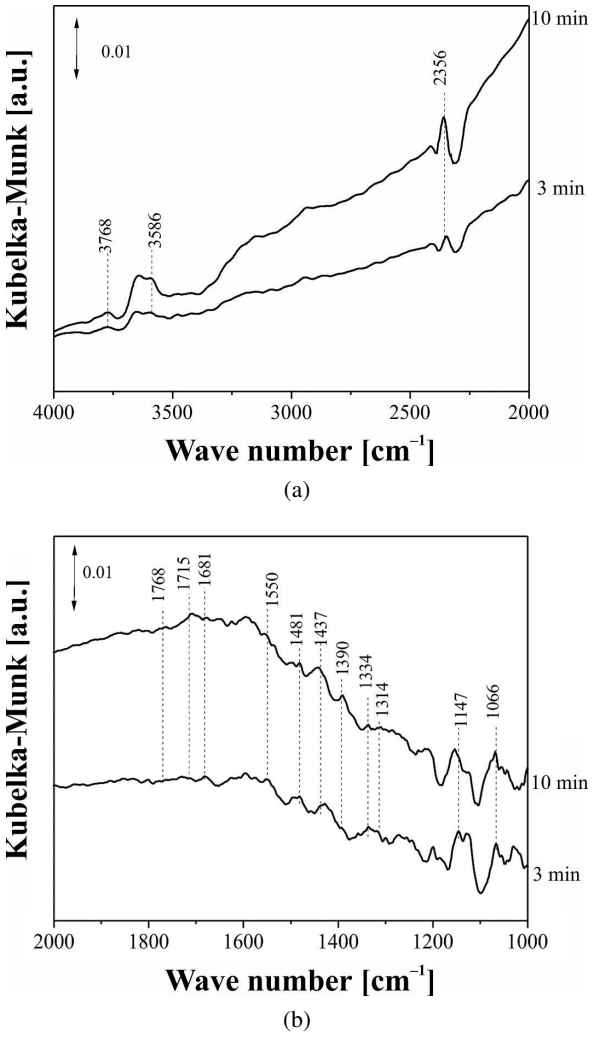

Fig. 4. DRFT-IR spectra of 200 ppm diethyl ether adsorption on an SnO_2 film and thermal decomposition of ethyl ether at 350 °C: (a) 4 000 cm^{-1} to 2000 cm^{-1}, (b) 2 000 cm^{-1} to 1 000 cm^{-1}.

Fig. 4 shows the DRFT-IR spectra of 200 ppm diethyl ether adsorption on SnO_2 film and thermal decomposition of ethyl ether at 350 °C. The absorption peaks at ν = 3768 cm^{-1}, 3586 cm^{-1} are the stretching vibration of H_2O molecule $\nu(H_2O)$; that at ν = 2356 cm^{-1} is a stretching vibration of CO_2, the intensity of CO_2 peak after 10 min is higher than that after 3 min. It indicates that the production of CO_2 progressively increased. And those at ν = 1768 cm^{-1}, 1715 cm^{-1} can be assigned as a C=O stretching vibration ν(C=O) of aldehyde (HCHO or CH_3CHO). The absorption band at ν = 1681 cm^{-1} is a C=C stretching vibration ν(C=C). The band at ν = 1550 cm^{-1} is the deformation vibration of a H_2O molecule $\delta(H_2O)$. And those at ν = 1481 cm^{-1} and 1390 cm^{-1} are CH_2, CH_3 deformation vibrations $\delta(CH_2)$, $\delta(CH_3)$, respectively. These bands can be attributed to the intermediate products ethyl ($CH_3CH_2\bullet$) and oxoethyl ($CH_3CH_2O\bullet$). The absorption peaks at ν = 1437 cm^{-1} and 1314 cm^{-1} are deformation vibrations $\delta(CH_2)$ and δ(CH) of ethylene (C_2H_4) molecule, and this means that C_2H_4 has been produced. That at ν = 1334 cm^{-1}

Table 1. IR assignments of diethyl ether adsorption on an SnO_2 film and thermal decomposition of ethyl ether at different temperatures.

Surface species	Wave number [cm^{-1}] (350 °C)	Wave number [cm^{-1}] (380 °C)	Wave number [cm^{-1}] (400 °C)	Literature
$\nu(H_2O)$	3768/3586	3768/3563/3210	3769/3513	[38]
$\nu(CO_2)$	2356	2347	2347	[39]
$\nu(C{=}O)$	1768/1715	1781/1723	1760/1710	[40]
$\nu(C{=}C)$	1681	1647	1649	[40, 41]
$\delta(H_2O)$	1550	3642/1591	1586	[42–44]
$\delta_a(CH_2)$	1481	1490	1523	[45–49]
$\delta_b(CH_2)$	1437	1409	1467	[45–49]
$\delta(-CH_3)$	1390	1386	1372	[42, 43]
ν(C–CHO)	1334	1462	1426	[42, 43]
δ(OH)	–	1336	1329	[42, 43]
δ(CH)	1314	1293	1218	[50, 51]
ν(C–O–C)	1147	1147	1164	[41]
ν(C–C)	1066	1052	1091	[50–52]
ν(C–O)	–	1026	1040	[45, 53]

Note:
$\delta_a(CH_2)$: $CH_3CH_2\bullet/CH_3CH_2O\bullet$
$\delta_b(CH_2)$:$CH_2 = CH_2$

is a C–CHO stretching vibration ν(C–CHO), and it suggests that HCHO and CH_3CHO have been produced [9, 48–54]. The absorption peak at $\nu = 1147\ cm^{-1}$ is a C–O–C stretching vibration ν(C–O–C) of diethyl ether, and this means that diethyl ether molecule has been absorbed on the surface. And that at $\nu = 1066\ cm^{-1}$ is a C–C stretching vibration ν(C–C).

Possible equations describing the process may be written as follows [54]:

$$CH_3CH_2OCH_2CH_3(g) \rightarrow CH_3CH_2OCH_2CH_3(ads) \quad (5)$$

$$CH_3CH_2OCH_2CH_3(ads) + SnO_2 \rightarrow CH_3CH_2\bullet + CH_3CH_2O\bullet + SnO_2 \quad (6)$$

$$CH_3CH_2\bullet \rightarrow C_2H_4 + H\bullet \quad (7)$$

$$CH_3CH_2O\bullet \rightarrow CH_3CHO + H\bullet \quad (8)$$

$$CH_3CH_2O\bullet \rightarrow HCHO + CH_3\bullet \quad (9)$$

$$C_2H_4 + 6O^- \rightarrow 2H_2O + 2CO_2 + 6e^- \quad (10)$$

$$CH_3CHO + 5O^- \rightarrow 2H_2O + 2CO_2 + 5e^- \quad (11)$$

$$HCHO + 2O^- \rightarrow H_2O + CO_2 + 2e^- \quad (12)$$

Fig. 5 shows DRFT-IR spectra of 200 ppm diethyl ether adsorption on the SnO_2 film and thermal decomposition of ethyl ether at the optimal temperature of 380 °C. Compared to Fig. 4, the peak intensities of CO_2 are enhanced and some new peaks are apparent. The peaks at $\nu = 3768\ cm^{-1}$, $3563\ cm^{-1}$ and $3210\ cm^{-1}$ are the stretching vibration of H_2O molecule $\nu(H_2O)$, those at $\nu = 3642\ cm^{-1}$ and $1591\ cm^{-1}$ are the deformation vibration of H_2O molecule $\delta(H_2O)$. And that at $\nu = 2347\ cm^{-1}$ is a CO_2 stretching vibration $\nu(CO_2)$. The intensity of the CO_2 peak after 10 min, at 380 °C, is also higher than that after 3 min. The absorption peaks at $\nu = 1781\ cm^{-1}$ and $1723\ cm^{-1}$ are C=O stretching vibration ν(C=O) of an aldehyde (HCHO or CH_3CHO). And that at $\nu = 1647\ cm^{-1}$ is a C=C stretching vibration ν(C=C). The peaks at $\nu = 1490\ cm^{-1}$ and $1386\ cm^{-1}$ are the CH_2, CH_3 deformation vibrations $\delta(CH_2)$, $\delta(CH_3)$, respectively. These features can be attributed to the

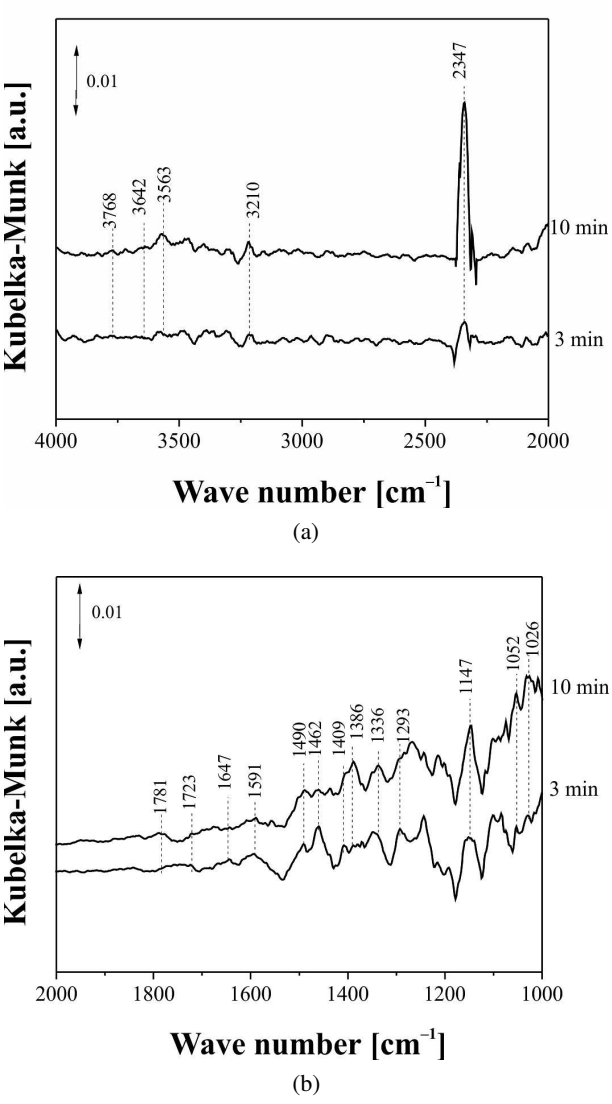

Fig. 5. DRFT-IR spectra of 200 ppm diethyl ether adsorption on an SnO_2 film and thermal decomposition of ethyl ether at 380 °C: (a) 4 000 cm^{-1} to 2 000 cm^{-1}, (b) 2 000 cm^{-1} to 1 000 cm^{-1}.

intermediate products ethyl (CH_3CH_2•) and oxoethyl (CH_3CH_2O•). And those at ν = 1409 cm^{-1} and 1293 cm^{-1} are deformation vibrations $\delta(CH_2)$ and δ(CH) of ethylene (C_2H_4) molecule. The absorption band at ν = 1462 cm^{-1} is a C–CHO stretching vibration ν(C–CHO). That at ν = 1147 cm^{-1} is a C–O–C stretching vibration ν(C–O–C) of diethyl ether. The absorption peak at ν = 1052 cm^{-1} is a C–C stretching vibration ν(C–C). And that at ν = 1026 cm^{-1} is C–O stretching vibration ν(C–O). New absorption peaks, compared to Fig. 4, that appear at ν = 1026 cm^{-1} comprise a C–O stretching vibration ν(C–O), at ν = 3210 cm^{-1} and 1336 cm^{-1} OH stretching vibration and deformation vibration ν(O–H), δ(O–H), respectively. The peaks at ν = 1386 cm^{-1} and 1336 cm^{-1} are the functional group –CH_3's characteristic absorption of ethyl alcohol molecule.

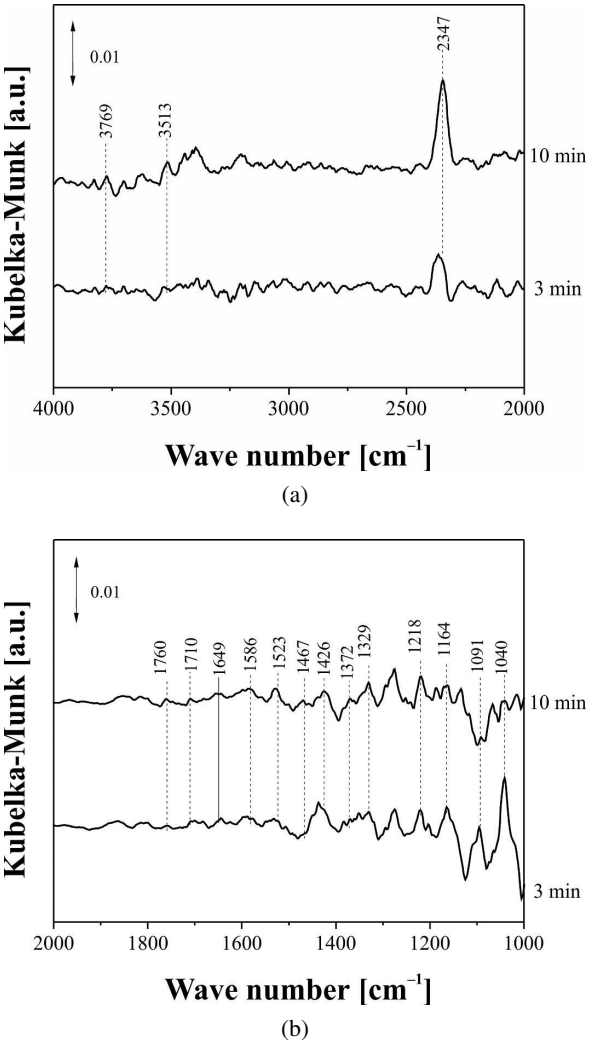

Fig. 6. DRFT-IR spectra of 200 ppm diethyl ether adsorption on an SnO_2 film and thermal decomposition of ethyl ether at 400 °C: (a) 4 000 cm^{-1} to 2 000 cm^{-1}, (b) 2 000 cm^{-1} to 1 000 cm^{-1}.

Fig. 6 shows DRFT-IR spectra of 200 ppm diethyl ether adsorption on the SnO_2 film and thermal decomposition of ethyl ether at 400 °C. The bands at ν = 3769 cm^{-1} and 3513 cm^{-1},

1586 cm^{-1} are the stretching and deformation vibrations of H_2O molecule $\nu(H_2O)$ and $\delta(H_2O)$. That at $\nu = 2347$ cm^{-1} is a CO_2 stretching vibration $\nu(CO_2)$. The absorption peaks at $\nu = 1760$ cm^{-1}, 1710 cm^{-1} are C=O stretching vibration ν(C=O) of aldehyde (HCHO or CH_3CHO). That at $\nu = 1649$ cm^{-1} is C=C stretching vibration ν(C=C). And those at $\nu = 1523$ cm^{-1} and 1372 cm^{-1} are the CH_2, CH_3 deformation vibrations $\delta(CH_2)$, $\delta(CH_3)$ of the intermediate products ethyl(CH_3CH_2•) and oxoethyl (CH_3CH_2O•). The bands at $\nu = 1467$ cm^{-1} and 1218 cm^{-1} are deformation vibration $\delta(CH_2)$ and δ(CH) of ethylene (C_2H_4) molecule, these features can all be assigned to the intermediate product C_2H_4. That at $\nu = 1426$ cm^{-1} is a C–CHO stretching vibration ν(C–CHO), and it indicates that HCHO and CH_3CHO have been produced. And those at $\nu = 1091$ cm^{-1} and 1329 cm^{-1} are C–C and O–H stretching vibration and deformation vibration ν(C–C) and δ(O–H). The absorption peak at $\nu = 1164$ cm^{-1} is a C–O–C stretching vibration ν(C–O–C) of diethyl ether. And that at $\nu = 1040$ cm^{-1} is a C–O stretching vibration ν(C–O).

A possible reaction mechanism of diethyl ether at 380 °C and 400 °C may be written using equation 5 to equation 12 as well as the following [54]:

$$CH_3CH_2OCH_2CH_3(ads) + SnO_2 \rightarrow CH_3CH_2OH + C_2H_4 + SnO_2 \quad (13)$$

$$CH_3CH_2OH + 6O^- \rightarrow 3H_2O + 2CO_2 + 6e^- \quad (14)$$

Fig. 7 shows DRFT-IR spectra of 200 ppm diethyl ether adsorption on the SnO_2 film and thermal decomposition of ethyl ether after 10 min at different temperatures. From Fig. 7, it can be seen that the CO_2 peaks at 380 °C are more intense than at 350 °C or 400 °C, the absorption peak at 380 °C near $\nu = 1026$ cm^{-1}, attributable to (C–O) of ethanol, is most intense at 380 °C, implying more ethanol production at this temperature. The bands attributable to (C–C) of CH_3CH_2• and CH_3CH_2O• are also more intense at 380 °C than at 350 °C or 400 °C. This result is consistent with

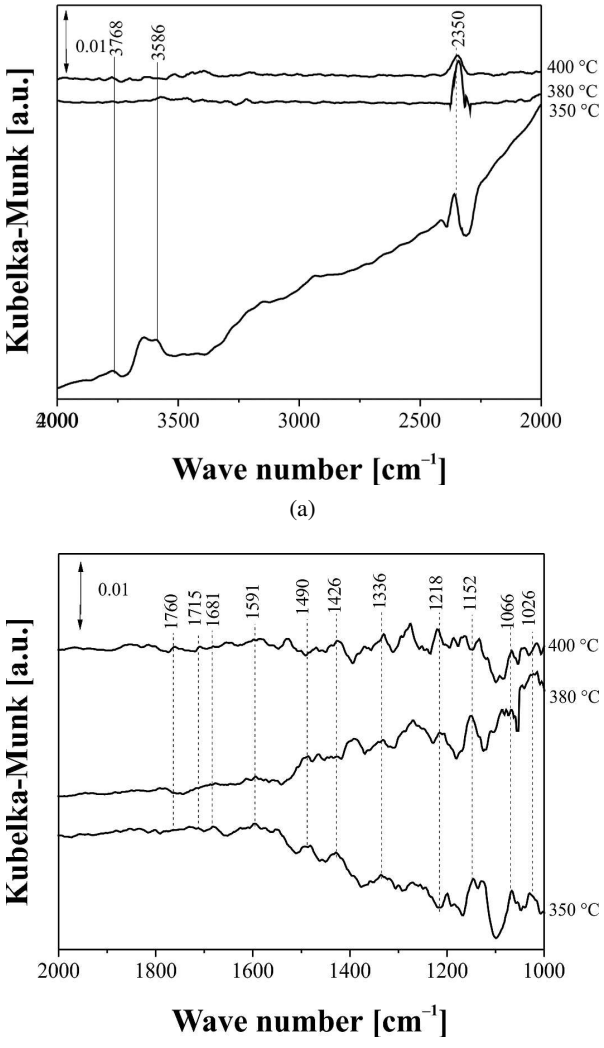

Fig. 7. DRFT-IR spectra of 200 ppm diethyl ether adsorption on an SnO_2 film and thermal decomposition of ethyl ether after 10 min at different temperatures: (a) 4 000 cm^{-1} to 2 000 cm^{-1}, (b) 2 000 cm^{-1} to 1 000 cm^{-1}.

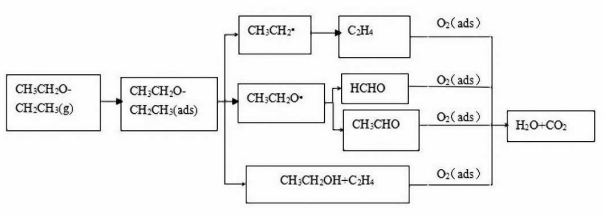

Fig. 8. Mechanism of diethyl ether adsorption and reactions on an SnO_2 film including partial thermal decomposition of ethyl ether and oxidation of decomposition products.

the change in the gas-sensing properties (Fig. 1), that is, the maximum amount of CO_2 is produced at 380 °C due to maximum diethyl ether absorption, and the gas sensitivity at 380 °C is accordingly the highest.

Based on the products identified by the DRFT-IR spectra under our experimental conditions (Fig. 4 to Fig. 6), we can speculate that when the SnO_2 film was exposed to diethyl ether, the molecules were initially adsorbed on its surface. The absorbed diethyl ether molecules then decomposed and generated intermediate products CH_3CH_2•, CH_3CH_2O•, CH_3CH_2OH and C_2H_4. These CH_3CH_2• and CH_3CH_2O• reacted further to produce C_2H_4, HCHO, and CH_3CHO. These intermediate products could further react with the oxygen anions on the surface generating H_2O and CO_2 as the reaction time increased from 3 min to 10 min. Thus, a simplified reaction scheme of diethyl ether molecules on the SnO_2 film including partial thermal decomposition of ethyl ether and the oxidation of decomposition products under our experimental conditions, as shown in Fig. 8, may be proposed. The reaction path is the same as that in literature reports [9, 33, 54, 55].

4. Conclusions

An SnO_2 diethyl ether gas sensor has been successfully fabricated by a screen-printing technique based on SnO_2 powder prepared by a sol-gel method. The gas sensitivity of the obtained SnO_2 sensor to 1 ppm and 200 ppm diethyl ether reached 2.19 and 113.03 at 380 °C, respectively. The results of DRFT-IR spectra revealed that ethyl (CH_3CH_2•), oxoethyl (CH_3CH_2O•), CH_3CH_2OH, HCHO, CH_3CHO, C_2H_4, H_2O, CO_2, and molecularly adsorbed diethyl ether surface species were formed during the interaction of diethyl ether with the SnO_2 film and thermal decomposition of ethyl ether at different temperatures. The mechanism of the reaction process may promote the development of improved gas sensors for diethyl ether, which may offer ultra-high detection capabilities for such organic molecules.

Acknowledgements

This work was supported by the Natural Science Foundation of Hubei Province, China (Grant No. 2014CFB1009), and the Opening Project (2015-KF-6) of the State Key Laboratory of Advanced Technology for Materials Synthesis and Processing (Wuhan University of Technology). The authors are also grateful to the Analytical and Testing Center of Huazhong University of Science and Technology.

References

[1] Chen G.Q., Wu Y.M., Zhu T., Zhang Y.Z., *J. Atom. Mol. Phys.*, 24 (2007), 101 (in Chinese).
[2] Rakopoulos D.C., Rakopoulos C.D., Giakoumis E.G., Dimaratos A.M., *Energy*, 43 (2012), 214.
[3] Bai C.H., Zhang B., Xiu G.L., Liu Q.M., Chen M., *Fuel*, 107 (2013), 400.
[4] Yuan X.L., Xie C.S., Yang L., Zhang S.P., *Sensor. Actuat. B-Chem.*, 195 (2014), 439.
[5] Liu J.Q., Zhang Y.T., Yuan Y.F., Zuo W.W., *Acta Chim. Sinica*, 71 (2013), 102.
[6] Cao X.P., *Forensic Sci. Technol.*, 4 (1981), 66 (in Chinese).
[7] Wang J., Dong C.R., *Chinese J. Practical Int. Med.*, 3 (1983), 252 (in Chinese).
[8] Scotter M.J., Roberts D.P.T., *J. Chromatogr. A*, 1157 (2007), 386.
[9] Hu J., Xu K.L., Jia Y.Z., Lv Y., Li Y.B., Hou X.D., *Anal. Chem.*, 80 (2008), 7964.
[10] Lin H.B., Shi J.S., *Sensor. Actuat. B-Chem.*, 92 (2003), 243.
[11] Cao X.A., Chen Z.H., Wang Y.L., *J. Guangzhou Uni. Nat. Sci. Ed.*, 9 (2010), 28 (in Chinese).
[12] Cao X.A., Wu W.F., Chen N., Peng Y., Liu Y.H., *Sensor. Actuat. B-Chem.*, 137 (2009), 83.
[13] Volanti D.P., Felix A.A., Orlandi M.O., Whitfield G., Yang D.J., Longo E., Tuller H.L., Varela J.A., *Adv. Funct. Mater.*, 23 (2013), 1759.
[14] Xie C.S., Xiao L.Q., Hu M.L., Bai Z.K., Xia X.P., Zeng D.W., *Sensor. Actuat. B-Chem.*, 145 (2010), 457.
[15] Li Y., Hsu P.C., Chen S.M., *Sensor. Actuat. B-Chem.*, 2012, 174 (2012), 427.
[16] Ohgaki T., Matsuoka R., Watanabe K., *Sensor. Actuat. B-Chem.*, 150 (2010), 99.
[17] Liu S.Q., Xie M.J., Li Y.X., Guo X.F., Ji W.J., Ding W.P., *Sensor. Actuat. B-Chem.*, 151 (2010), 229.
[18] He L.F. He, Guo Z., Chen X., Meng F.L., Luo T., Li M.Q., Liu J.H., *J. Phys. Chem. C*, 113 (2009), 9581.
[19] Wang D., Chu X.F., Gong M.L., *Sensor. Actuat. B-Chem.*, 117 (2006), 183.
[20] Hyodo T., Abe S., Shimizu Y., Egashira M., *Sensor. Actuat. B-Chem.*, 93(2003), 590.
[21] Huang J., Matsunaga N., Shimanoe K., Yamazoe N., Kunitake T., *Chem. Mater.*, 17 (2005), 3513.
[22] Wang P.J., Yao B.H., Wei Q.B., Zhang Y.Q., Xue H.F., *Chem. Bioeng.*, 29 (2012), 21 (in Chinese).

[23] REN Y.F., *J. Chinese Soc. Rare Earth*, 3 (1985), 15 (in Chinese).
[24] SLOBODIAN P., RIHA P., LENGALOVA A., SVOBODA P., SAHA P., *Carbon*, 49 (2011), 2499.
[25] MA X.D., GUO H., GUO X., LV L., HE X., FENG X., *Chem. J. Chinese U.*, 33 (2012), 1915.
[26] ZHAO W., ZHANG Z.Y., WU T.Z., WANG X.W., DENG Z.H., DAI K., *Electron. Comp. Mater.*, 24 (2005), 36 (in Chinese).
[27] AIZAWA H., NODA K., NAGANAWA R., YAMADA K., YOSHIMOTO M., REDDY S. M., KUROSAWA S., *J. Photopolym. Sci. Tec.*, 22 (2009), 743.
[28] GUI Y.H., CUI R.L., NIU L.J., *Conserv. Util. Miner. Resour.*, 6 (2009), 32 (in Chinese).
[29] HUANG K.J., ZHANG Z. X., YUAN F. L., XIE C. S., *Curr. Nanosci.*, 9 (2013), 357.
[30] WANG X. J., ZHANG S. P., ZHANG G. Z., *Electron. Technol.*, 39 (2012), 53 (in Chinese).
[31] ZHANG H., FENG J. C., FEI T., LIU S., ZHANG T., *Sensor. Actuat. B-Chem.*, 190 (2014), 472.
[32] ZHANG Z.X., HUANG K.J., YUAN F.L., XIE C. S., *J. Mater. Res.*, 29 (2014), 139.
[33] LIU X.M., ZHANG Q., ITO S., WADA Y., *Fuel*, 165 (2016), 513.
[34] YIN L., CHEN D. L., CUI X., GE L. F., YANG J., YU L.L., ZHANG B., ZHANG R., SHAO G. S., *Nanoscale.*, 6 (2014), 13690.
[35] LEE S. K., CHANG D., KIM S.W., *J. Hazard. Mater.*, 268 (2014), 110.
[36] SUCHORSKA-WOZNIAK P., RAC O., FIEDOT M., TETERYEZ H., *Sensors-Basel*, 14 (2014), 20480.
[37] ZHANG Z.Y., ZOU R.J., SONG G.S., YU L., CHEN Z. G., HU J.Q., *J. Mater. Chem.*, 21 (2011), 17360.
[38] GROSSMANN K., PAVELKO G.R., BARSAN N., *Sensor. Actuat. B-Chem.*, 166 (2012), 787.
[39] YOKOSUKA Y., OKI K., NISHIKIORI H., *Res. Chem. Intermediat.*, 35 (2009), 43.
[40] JANG M., MCDOW S.R., *Environ. Sci. Technol.*, 31 (1997), 1046.
[41] HUANG S.Y., ZHANG C.B., HE H., *Catal. Today*, 139 (2008), 15.
[42] HU J.H., ZHENG X.F., *Practical Infrared Spectroscopy*, Science Press, Beijing, 2011 (in Chinese).
[43] FENG J.C., *Structural Analysis and Identification of Organic Compounds*, National Defence Industry Press, Beijing, 2003 (in Chinese).
[44] WENG S.F., *Fourier Transform Infrared Spectrum Analysis*, Chemical Industry Press, Beijing, 2010 (in Chinese).
[45] KECSKES T., RASKO J., KISS J., *Appl. Catal. A-Gen.*, 273 (2004), 55.
[46] XU W.Z., RAFTERY D.S.J., *J. Phys. Chem. B*, 107 (2003), 4537.
[47] DU X., DU Y., GEORGE S.M., *J. Phys. Chem. A*, 112 (2008), 9211.
[48] MILLAR J.G., COLIN H., ROCHESTER H.C., *J. Catal.*, 155 (1995), 52.
[49] HE Y.B., JI H.B., *Chinese J. Catal.*, 31 (2010), 171.
[50] DRIESSEN M.D., GOODMAN A.L., MILLER T.M., *J. Phys. Chem. B*, 102 (1998), 549.
[51] FAN J.F., JOHN T.Y., *J. Am. Chem. Soc.*, 118 (1996), 4686.
[52] KIM J.S., ITOH K., MURABAYASHI M., *Chemosphere*, 36 (1998), 483.
[53] RASKO J., KECSKES T., KISS J., *J. Catal.*, 226 (2004), 183.
[54] YASUNAGA K., GILLESPIE F., SIMMIE J.M., CURRAN H.J., KURAGUCHI Y., HOSHIKAWA H., YAMANE M., HIDAKA Y., *J. Phys. Chem. A*, 114 (2010), 9098.
[55] FARKAS A.P., SOLYMOSI F., *Surf. Sci.*, 602 (2008), 1497.

Received 2016-04-22
Accepted 2017-02-05